

Influence of synchrotron self-absorption on the 21cm experiments

Qian Zheng^{1,2,3}, Xiang-Ping Wu¹, Jun-Hua Gu¹, Jingying Wang⁴, Haiguang Xu⁴

¹*National Astronomical Observatories, Chinese Academy of Sciences, Beijing 100012, China; Email: zq@bao.ac.cn*

²*LERMA, Observatoire de Paris, 61, Avenue de l'Observatoire, 75014, Paris, France*

³*Graduate School of Chinese Academy of Sciences, Beijing 100049, China*

⁴*Department of Physics, Shanghai Jiao Tong University, 800 Dongchuan Road, Shanghai 200240, China*

Received date / accepted date

ABSTRACT

Presence of spectral curvature due to synchrotron self-absorption of extragalactic radio sources may break down the spectral smoothness feature - the premise that bright radio foreground can be successfully removed in the 21cm experiments of searching for the epoch of reionization (EOR). We present a quantitative estimate of the effect on the measurement of the angular power spectrum of the low-frequency sky, incorporating a phenomenological model, characterized by the fraction (f) of radio sources with turnover frequencies in 100-1000 MHz range and a broken power law for the spectral transition around turnover frequencies ν_m , into the simulated radio sources over a small sky area of $10^\circ \times 10^\circ$. We compare statistically the changes in their residual maps with and without inclusion of the synchrotron self-absorption of extragalactic radio sources after the bright sources of $S_{150\text{MHz}} \geq 100$ mJy are excised and the best-fitted polynomials in frequency domain on each pixel are further subtracted. It has been shown that the effect of synchrotron self-absorption on the detection of EOR depends sensitively on the spectral profiles of radio sources around the turnover frequencies ν_m : A hard transition model described by the broken power law with the turnover of spectral index at ν_m would leave pronounced imprints on the residual background and therefore cause serious confusion with the cosmic EOR signal. However, the spectral signatures on the angular power spectrum of extragalactic foreground generated by a soft transition model, in which the rise and fall power laws of spectral distribution around ν_m are connected through a smooth transition spanning ≥ 200 MHz in characteristic width, can be fitted and consequently subtracted by employment of polynomials to an acceptable degree ($\delta T < 1$ mK). As this latter scenario seems to be favored by both theoretical expectation and radio spectral observations, we conclude that the contamination of extragalactic radio sources of synchrotron self-absorption in the 21cm experiments is probably very minor.

Key words: cosmology: theory — cosmology: observations — diffuse radiation — intergalactic medium — radio lines: galaxies

1 INTRODUCTION

While the redshifted 21cm neutral hydrogen emission is believed to be the most promising tool in the probe of the epoch of reionization (EOR) and the dark ages, the signal from the high-redshift universe is deeply buried under the extremely bright foreground dominated by our Galaxy and extragalactic sources. An unprecedented level of foreground removals down to 5 orders of magnitude should therefore be required to 'excavate' the cosmic signal even in a statistical manner such as the employment of power spectrum (for recent reviews see Furlanetto, Peng Oh & Briggs 2006; Morales & Wyithe 2010; Pritchard & Loeb 2011). Yet, it is generally agreed among the 21cm cosmology community that the foregrounds at low frequencies should exhibit a featureless spectrum as a result of the spectral smoothness of the synchrotron and free-free emission, and subtracting a smooth component characterized usually by a power-law or polynomial in frequency domain from the redshifted

21cm observations should allow one to remove the foreground contamination to a desired degree. Moreover, such an algorithm can be performed in either the visibility (uv) space (Zaldarriaga, Furlanetto & Hernquist 2004; Liu et al. 2009; Harker et al. 2010; etc.) or the image space (Furlanetto, Zaldarriaga & Hernquist 2004; Santos, Cooray & Knox 2005; Wang et al. 2006; Di Matteo, Ciardi & Miniati 2004; etc.), and even directly for the angular power spectrum (Ghosh et al. 2011a,b; Cho, Lazarian & Timbie. 2012). It is, of course, essential that all bright sources in the field of view should be successfully excised before the subtraction to both ensure a large dynamical range ($\sim 10^5$) and reduce the shot noise arising from their Poisson distribution. In other words, the foreground removals deal primarily with the unresolved foreground sources.

Indeed, in our interested low frequency range, say from 50 MHz to 200 MHz, corresponding to 21cm neutral hydrogen line at redshifts between 6 and 27, a power-law or polynomial provides an accurate approximation of the spectral distribution for most cases of extragalactic radio sources. However, it has been known for several decades that some of the extragalactic radio sources including galaxies, QSOs and even clusters of galaxies exhibit curvatures in their spectral distributions, manifested by the change in their spectral indices approaching a constant value of 2.5 below the so-called cutoff or turnover frequency (e.g. Kellermann & Pauliny-Toth 1969; Laing & Peacock 1980; Andernach, Waldthausen & Wielebinski 1980; Hodges, Mutel & Phillips 1984). A natural and also widely accepted explanation for the spectral curvature is the synchrotron self-absorption (Pacholczyk 1970; Tsvetanov & Charugin 1981), though other mechanisms such as inverse Compton loss and free-free absorption or their combination may partially contribute to the phenomenon. For any given wavebands particularly in the low frequency range, the fraction of the extragalactic radio sources with spectral curvature is very uncertain. In their early work, Kellermann & Pauliny-Toth (1969) compiled 30 radio sources that show strong evidence of spectral curvature with turnover frequencies from ~ 10 MHz to ~ 1 GHz. Steppe et al. (1995) observed 76 radio sources at millimeter wavelength and found about 5 sources whose turnovers occur at frequencies below 1 GHz. Probably these two observations would give us a sense that the fraction of the radio sources with turnover frequencies below 1 GHz is not negligibly small.

Although a number of newly proposed algorithms for foreground removals do not necessarily depend on the assumption of spectral smoothness of the foregrounds (e.g. Harker et al. 2009; Harker et al. 2010; Chapman et al. 2012), here we would still concentrate on the conventional method which makes an attempt at fitting and subtracting a polynomial of the form $\log T_{\text{fit}} = \sum_{i=0}^{N_{\text{poly}}} a_i \log(\nu/\nu_0)^i$ to the observation in either image space or Fourier (uv) space, where N_{poly} is the order of polynomial and ν_0 is a characteristic frequency (e.g. Wang et al. 2006; Jelić et al. 2006; Pritchard & Loeb 2010). We have chosen the $\log(T) - \log(\nu)$ polynomial rather than the $T - \nu$ form for convenience, and the two forms of polynomial yield essentially similar result (Petrovic & Peng Oh 2011). The overall shape of the best-fit polynomial is governed by a_1 , the leading component of power index, and the remaining high order terms for $i \geq 2$ provide only a minor correction to the deviation of power index from the dominant one a_1 . With the best-fit parameter $a_1 < 0$ for the integrated foreground of extragalactic radio sources in low frequency range of $50 \text{ MHz} \leq \nu \leq 200 \text{ MHz}$, the commonly adopted form of polynomial describes actually a monotonically decreasing function of ν . Although it was claimed that the foreground is not perfectly flat due to synchrotron self-absorption, it is believed that the current fitting and subtracting techniques are still able to filter out the slowly varying foreground along the line of sight (Morales & Wythe 2010). Yet, to what extent the contamination of radio sources with spectral curvature in the 21cm experiments can be eliminated has actually remained unclear so far. At least there has been no quantitative estimate of this particular effect in the literature. It seems likely that any spectral structures of foreground sources after performing the fitting and subtraction of a polynomial would be treated as residuals, which could mimic or cause confusion with the cosmic EOR signal.

In this paper we demonstrate quantitatively the effect of spectral curvature of extragalactic radio sources as a result of synchrotron self-absorption on the evaluation of the angular power spectrum of low-frequency sky. This is achieved by comparing the angular power spectra of the redshifted 21cm sky with and without the inclusion of spectral curvature for extragalactic radio sources after the same method of foreground removals is employed. Our radio foreground is constructed from the simulation of Wilman et al. (2008) with a modification of power index for the radio sources of spectral curvature, whereas the fraction of the radio sources of synchrotron self-absorption in a given waveband remains to be a free parameter. We work straightforwardly in the image space furnished by the numerical simulation containing no EOR signal at all, with emphasis only on the effect of spectral curvature on foreground removals. Throughout this paper we assume the concordance cosmological model (Λ CDM) with the following choice of cosmic parameters: $\Omega_M = 0.27$, $\Omega_\Lambda = 0.73$, $\Omega_b h^2 = 0.0224$, $h = 0.71$, $n_s = 0.93$ and $\sigma_8 = 0.84$.

2 EXTRAGALACTIC FOREGROUNDS

There have been many theoretical explorations both analytically and numerically in recent years on modeling of the redshifted 21cm foregrounds (e.g. de Oliveira-Costa et al. 2008; Jelić et al. 2008; Bowman, Morales & Hewitt 2009; Singal et al. 2010; Vernstrom et al. 2011; Liu & Tegmark 2011). We adopt the simulated low-frequency sky by Wilman et al. (2008), in which the observed luminosity functions of radio sources are incorporated with the underlying cosmic dark matter density field out to redshift of $z=20$. A total of five distinct radio source types are included in their semi-empirical simulation: radio quiet AGNs,

FRI and FRII AGNs, quiescent star-forming galaxies and star bursting galaxies. About 320 million sources down to 10 nJy are identified in a sky field of $20^\circ \times 20^\circ$ at five wavebands ranging from 151 MHz to 18 GHz.

We extract our source catalog from the $S^3 - SEX$ database generated by Wilman et al. (2008) over a smaller sky area of $10^\circ \times 10^\circ$. We estimate the flux of each radio source at different observing frequencies between 100 MHz and 200 MHz by extrapolating its corresponding value at 5 GHz in terms of a single power-law of ν^α if no spectral curvature is concerned. Unlike Wang et al. (2010) who took into account the variation of power index for each type of radio sources in the conversion of flux at different frequencies, we simply assume a power index of $\alpha = -0.75$ for AGNs including FRI and FRII types and $\alpha = -0.7$ for star forming/bursting galaxies. The final catalog contains 74 million sources, and only 0.8% of them have fluxes greater than 100 mJy at 150 MHz which are named 'bright' or resolved sources in this work and will be excised later. In other words, 99.2% of the sources will be treated as the 'unresolved' foregrounds. The simulated intensity map of these 'unresolved' sources with fluxes fainter than 100 mJy is displayed in Fig. 1, in which the image has been smoothed using a Gaussian kernel of FWHM = $1'.98$, corresponding to a radio array with a baseline of 5 km. We will adopt this angular resolution, $1'.98(\nu/150\text{MHz})^{-1}$, for the simulated sky maps at other frequencies.

We have extensively searched the literature to collect as many as possible the radio sources of spectral curvature due to synchrotron self-absorption, in an attempt to find whether there are any correlations between the turnover frequencies ν_m and other observables such as the total flux, the maximum flux S_{max} or the fluxes at particular frequencies. The purpose is to insert a more realistic model of synchrotron self-absorption into the above simulation by allocating the proper turnover frequencies to the sources of spectral curvature in terms of known or observed quantities. Unfortunately, we failed in establishing any statistically meaningful relationships including the expected dependence of S_{max} on ν_m within the framework of synchrotron self-absorption under the assumption of a constant magnetic field B : $S_{\text{max}} \propto \nu_m^{5/2} B^{-1/2}$. Fig. 2 shows the peak luminosities P_{max} , corresponding to S_{max} after the correction of cosmic expansion, against $\nu_m(1+z)$ for 39 sources (14 galaxies + 25 AGNs) with observing cutoff frequencies below 1 GHz compiled from three observations made by Kellermann & Pauliny-Toth (1969), Hodges et al. (1984) and Steppe et al. (1995). Although P_{max} seems to have a weak increasing trend with turnover frequencies $\nu_m(1+z)$, the actual application of the relation in construction of the synchrotron self-absorption model turns to be difficult due to poor statistics and large scatters. For example, a 95% confidence interval of the best-fit spectral index for the $P_{\text{max}} - \nu_m$ relation is in the range of 0.14 – 1.39. This probably indicates that magnetic fields demonstrate significant variations among radio sources.

Keeping in mind the weak dependence, if any, of ν_m on other observables, we incorporate the synchrotron self-absorption feature into the simulated radio source catalog from the $S^3 - SEX$ database simply by specifying the fraction of radio sources of spectral curvatures in a given frequency range while the sources of self-absorption are chosen randomly and their turnover frequencies follow a uniform distribution over the waveband. This is consistent with the observational claim that the turnover frequency may occur anywhere over the frequency range of observations (e.g. Kellermann & Pauliny-Toth 1969). We set a waveband of 100-1000 MHz in the restframe of the sources to include all the sources out to redshifts $z = 4$ for our interested observing frequency range of 100-200 MHz. Once a source in the catalog is chosen to be of spectral curvature in 100-1000 MHz, its spectral index below the cutoff frequency ν_m will be set to asymptotically approach 2.5. An immediate consequence of such a turnover of spectral index is that the radio flux of the source would drop dramatically with decreasing frequency below $\nu_m(1+z)$. This may explain the recent PAPER measurement at 145 MHz that among the ~ 500 identified sources the only source, 0008-412, with spectral turnover at ~ 500 MHz shows no counterpart to the 408-MHz Molonglo Reference Catalog (Jacobs et al. 2011). Therefore, inclusion of synchrotron self-absorption alters both the overall spectral index and brightness of the low-frequency radio sky.

Instead of invoking a sophisticated model for the spectral transition of radio source around the cutoff frequency ν_m within the framework of synchrotron self-absorption, we assume an analytic profile for the sake of simplicity: A broken power law of $\nu^{2.5}$ and $\nu^{-|\alpha|}$ is used to characterize the asymptotic spectral profile at $\nu \ll \nu_m$ and $\nu \gg \nu_m$, respectively. To avoid a sudden change of spectral index across ν_m , a soft or smooth transition around ν_m is accomplished by two parabola curves which match asymptotically with the power law at each side of the turnover frequency ν_m . The third parameter, in addition to the peak flux S_{max} and turnover frequency ν_m , is required in such model: the characteristic frequency width w , defined as the frequency difference between the two points at which the slope of each parabola is equal to that of the corresponding asymptotic power law. A visual examination of the available spectral distributions of the radio sources of synchrotron self-absorption (Kellermann & Pauliny-Toth 1969; Hodges et al. 1984 and Steppe et al. 1995) reveals that a typical value of w takes a few hundreds of MHz. We choose an extreme value of $w = 0$, called the hard transition model, to maximize the influence of spectral curvature, and a 'conservative' value of $w = 200$ MHz, called the soft transition model, to provide a more realistic estimate of the effect of synchrotron self-absorption on the foreground. Fig. 3 shows an example of the hard transition model and of the soft transition model of $w = 200$ MHz at $\nu_m = 200$ MHz, respectively, in which the peak flux is assumed to be $S_{\text{max}} = 1$ Jy for the latter. Intuitively, the soft transition model seems to provide a more natural and reasonable description for the spectral turnover in the process of synchrotron self-absorption, and the discontinuously sharp peak at ν_m in the hard transition model turns to be difficult to handle and filter out.

Now, the last free parameter in our model of synchrotron self-absorption is the fraction or percentage, f , of radio sources

with turnover frequencies in the waveband of 100-1000 MHz. Because very little is known about the constraint on f in terms of current radio observations, we work with three choices of f , covering the 'extreme' value of 10%, the moderate case of 1%, and the lower, probably more realistic value of 0.1%. Finally, the case of no spectral curvature ($f = 0\%$) serves as our fiducial model for comparison. Fig. 4 shows the average surface brightness temperature of our simulated maps of $10^\circ \times 10^\circ$ versus frequencies for the four choices of f , together with the residual after the best-fitted polynomial of $N_{\text{poly}} = 3$ over the whole frequency range from 100 MHz to 200 MHz is subtracted. We demonstrate the results for the hard transition model only, which gives rise to a maximum estimate of the effect of spectral curvature on the global 21cm sky intensity. It appears that except for the slightly lower amplitudes for $f > 0$ as a result of synchrotron self-absorption, the overall sky temperatures show no significant difference in shape as compared with the result of our fiducial model of $f = 0$. This allows us to subtract the foregrounds with and without inclusion of synchrotron self-absorption to essentially the same level as shown in Fig.4, in which the residuals reflect actually the current accuracy level of our foreground removals based on the polynomial fitting method. Indeed, the effect of spectral curvature has become insignificant by ensemble-averaging of surface brightness temperature over the sky. Consequently, the experiments of searching for the global EOR signatures such as EDGES (Bowman, Rogers & Hewitt 2007; Bowman & Rogers 2010) may be unaffected by the presence of foreground radio sources of synchrotron self-absorption.

3 ANGULAR POWER SPECTRUM

3.1 Foreground removals and shot noise

As our focus is not on the study of foreground removal techniques, we apply directly the pixel-by-pixel algorithm of Wang et al. (2006) for subtraction of the simulated extragalactic sources. Before we perform the foreground removal, there are two critical assumptions that we have to make. First, all the bright sources of flux greater than 100 mJy have been successfully excised. Second, thermal noise on each pixel has already been reduced to an acceptable degree. Yet, the first assumption or operation by no means implies that the shot noise due to the Poisson distribution of extragalactic sources has been reduced to the desired level for the detection of EOR signal. Rather, we will actually deal with the shot noise produced by the 'unresolved' extragalactic foregrounds. As for the second condition the thermal noise can in principle be reduced by both accumulating observations and/or employing statistical methods such as power spectrum, provided that the noises on different pixels are independent.

To guarantee a sufficiently large dynamical range of the foreground removal algorithm, we adopt a short frequency range of 20 MHz rather than the full frequency width of 100 MHz in the fitting of a log-log polynomial. Consequently, a set of five log-log polynomials, with a bandwidth of 20 MHz for each, are separately fitted to and then subtracted from the intensity on each pixel of the simulated backgrounds. We fix a 1024^2 grid to sample the simulated image with a size of $10^\circ \times 10^\circ$, which gives rise to an angular resolution of $0.''6$. Here we have included no any instrumental responses such as frequency-dependent field-of-view and angular resolution to lay stress only on the effect of the spectral curvature of extragalactic radio sources.

Even without inclusion of the noises from telescope system and the Milky Way, the angular power spectrum of the radio sky at a given low-frequency is still dominated by the shot noise of the 'unresolved' extragalactic sources, as demonstrated in Fig. 5 for four frequency channels. Such Poisson noise is fully characterized by the differential source counts dN/dS below the flux cut S_{cut} (see Knox et al. 2001; Di Matteo et al. 2002): $C_\ell^{\text{shot}} = \int_0^{S_{\text{cut}}} S^2 (dN/dS) dS$. Given the fact that the cosmological signal from EOR has a brightness temperature fluctuation of a few to ten mK (e.g. Zaldarriaga et al. 2004), the shot noise power spectrum of the foregrounds consisting of the 'unresolved' sources below S_{cut} should be further and blind suppressed by at least two orders of magnitude in order to extract statistically the EOR information. This is accomplished by various foreground removal techniques including the polynomial fitting algorithm. It should be pointed out that the angular power spectrum constructed from our simulated sky is restricted within a narrow multipole range roughly from $\ell \approx 20$ to $\ell \approx 1000$ due to the small field of $10^\circ \times 10^\circ$ and the smoothing window of $\text{FWHM} = 1'.98(\nu/150\text{MHz})^{-1}$. The former yields a large cosmic variance at smaller ℓ , while the latter smears out the spatial structures at larger ℓ . We will not account for these measurement errors in our calculation of power spectrum because they do not alter our conclusions to be drawn below.

3.2 Comparisons of angular power spectra: hard transition model

We now work with the residual map at each frequency after the best-fitted polynomials of $N_{\text{poly}} = 3$ are subtracted on each pixel. We first demonstrate the results for the hard transition model of spectral curvature. Fig. 6 displays the average surface brightness temperature of the residual maps for four choices of f , the fraction of radio sources of turnover frequencies in the 100-1000 MHz range. The difference between the residuals in Fig.4 and Fig.6 is as follows: the former is obtained by performing the polynomial fitting and subtraction on the global surface temperature after summing over the contribution of each pixel, whereas for the latter the polynomial fitting and subtraction are made on each pixel before the averaging. Regardless of the regular oscillation patterns in Fig.6 which are the consequences of the polynomial subtraction, the overall residuals of our fiducial model ($f = 0\%$) without synchrotron self-absorption are well below 0.1 mK in the entire frequency range of 100-200

MHz, indicating the success of the polynomial fitting and subtraction techniques in the removal of extragalactic radio sources. However, the average residual temperature rises with increase of the fraction parameter f , and some of the oscillation peaks exceed 1 mK in the case of $f \geq 1\%$. Because the average residual temperature at each frequency is somehow equivalent to the normalization factor of the corresponding angular power spectrum to be constructed, the large amplitude of the residual temperature of up to ~ 1 mK due to the presence of synchrotron self-absorption may challenge the statistical extraction of the EOR signal which is expected to have a maximum spatial variance of 1-10 mK. Furthermore, it is anticipated that the amplitudes of the angular power spectra at different frequencies may demonstrate significant variations as a result of the dramatic rise and fall of their normalizations as shown in Fig.6.

The angular power spectrum of the residual temperature map after subtraction of the best-fitted polynomials can be obtained straightforwardly at each frequency channel for the hard transition mode of $w = 0$. We plot in Fig. 7 the corresponding results, represented by $\delta T = [\ell(2\ell + 1)C_\ell/4\pi]^{1/2}$, for the four choices of f and frequency parameters used in Fig. 4. While the overall power spectra maintain roughly the same shape for the four models of f and at different frequencies, the amplitudes of the power spectra for all the three choices of $f \geq 0.1\%$ greatly exceed those from our fiducial model of $f = 0$. In most cases the amplitude differences can span three orders of magnitude, accounting for a power of up to a few - tens mK for $20 < \ell < 1000$ on the power spectrum of the radio sky. In other words, the shot noises from the foreground residuals are comparable to and thus capable of confusing the cosmic EOR signal, if the fraction of the extragalactic radio sources of spectral curvature in 100 – 1000 MHz is not less than 0.1%. Indeed, the presence of synchrotron self-absorption described by the hard transition model has already broken the spectral smoothness feature of extragalactic radio sources - a key assumption to beat down the extremely bright foregrounds in the 21cm experiments. It is also important to note that both the oscillation patterns along frequency direction (Fig.6) and the angular power spectra of the unresolved radio foregrounds in the existence of synchrotron self-absorption look very much similar to the EOR signatures, making the two phenomena practically indistinguishable.

Probably, an intuitive way to reduce the impact of extragalactic sources of spectral curvature in the framework of the hard transition model on the radio foregrounds is to adopt a lower flux threshold of $S_{\text{cut}} < 100$ mJy. Namely, one can identify and excise much fainter extragalactic radio sources to suppress further the flux level of the 'unresolved' foreground. Towards this end, we set S_{cut} down to an extremely low flux of 0.1 mJy at 150 MHz and assume that all bright sources above 0.1 mJy can be perfectly removed with existing and developing observational techniques such as CLEAN and its variants (e.g. Schwab 1984; Cotton & Uson 2008), peeling (Noordam 2004; van der Tol et al. 2007; Intema 2009), algebraic forward modeling (Bernardi et al. 2011), etc.. We have applied this fainter flux limit to the same source catalog compiled above and repeated all the computations. It turns out that the overall amplitudes of the resultant average surface brightness temperature and angular power spectra of the residual maps indeed decrease moderately as compared with the corresponding quantities in Figs 6 and 7. However, some part of the angular power spectra can still maintain high powers of up to a few mK especially at large ℓ in the case of $f > 0.1\%$, indicating the inefficiency of eliminating entirely the effect of spectral curvature on the foreground removals even down to the level of $S_{\text{cut}} = 0.1$ mJy. At such a lower flux threshold, the amplitude of the angular power spectrum for $f = 0$ is mainly governed by the noise resulting from polynomial fitting and subtraction, whereas the failure of removing the spectral oscillation structures with polynomial fitting for the radio sources of synchrotron self-absorption accounts for the relatively large amplitudes of their power spectra. Of course, one may adopt even smaller values of S_{cut} to continue the above procedure until the amplitude of the angular power spectrum is made below 1 mK, if the feasibility of radio observations and subtraction of very faint point sources are left aside. Note that the average flux and angular power spectrum of the radio sky, rather than their residuals, vary as $\langle S \rangle \propto S_{\text{cut}}^{2-|\alpha|}$ and $C_\ell^{\text{shot}} \propto S_{\text{cut}}^{3-|\alpha|}$, respectively. At the faint flux end, the spectral index α is approximately -1 . Consequently, one is in principle able to suppress both global flux and spatial structures of the foregrounds by imposing a lower flux cutoff on extragalactic sources. Yet, an extremely or even unreasonably lower flux threshold S_{cut} would be required to bring the foreground down to the level of cosmic EOR signal.

3.3 Comparisons of angular power spectra: soft transition model

It is very likely that the influence of synchrotron self-absorption of foreground radio sources on the 21cm experiments has been exaggerated by the oversimplified, hard transition model for spectral turnover, in which the discontinuously sharp peak at ν_m can hardly be filtered out through subtracting a set of polynomials. In other words, the excess power in the angular power spectrum of radio foreground in the case of $f \neq 0$ shown in Figs 6 and 7 could be an artifact of the spectral transition model. It is essential to use the soft transition model to clarify the issue. Indeed, in our soft transition model the smooth transition region around turnover frequency ν_m spans $w = 200$ MHz in frequency (see Fig.3), which is wider than the bandwidth of 20 MHz used in the polynomial fitting. Such a smooth component around ν_m should therefore be characterized by the polynomials and subtracted subsequently, if the overlapping parts of the rise and fall power laws around ν_m from different sources of spectral curvature are not serious.

Following the same procedure as for the hard transition model above, we display in Figs 8 and 9 the average surface brightness temperature and angular power spectra of the residual surface temperature maps for the soft transition model of $w = 200$ MHz with $S_{\text{cut}} = 100$ mJy at 150 MHz. It appears that both quantities are roughly one order of magnitude smaller

than the ones for the hard transition model, bringing the amplitudes of angular power spectra down to $\delta T \lesssim 1$ mK for the three choices of $f \neq 0$. Only in the case of low frequency $\nu = 110$ MHz can a slightly higher power of $\delta T \sim 1$ mK be seen for $f = 10\%$ and $\ell \geq 600$. This indicates that the influence of spectral curvature of radio sources on foreground removals is only moderate for $f \geq 10\%$ and at low frequencies $\nu \lesssim 110$ MHz, and becomes actually minor for frequencies beyond $\nu \gtrsim 125$ MHz. Most likely, the characteristic width w would not be smaller than 200 MHz in terms of available spectral observations of radio galaxies and the fraction of radio sources of spectral curvature in the 100-1000 MHz range would not exceed $f = 10\%$ as indicated by existing samples such as Kellermann & Pauliny-Toth 1969 and Steppe et al. 1995. Therefore, the actual angular power spectra of foreground residual maps probably have their amplitudes well below 1 mK if a large value of w and a smaller value of f parameters are taken.

Such an apparent contradiction between the results of the hard transition model and the ones of the soft transition model with $w \geq 200$ MHz emphasizes the importance of understanding and properly modeling the spectral properties of radio sources in the 21cm experiments. Any sharp, though weak, variations in spectral distributions of foreground radio sources over a narrow band might leave observing imprints on the foreground residuals, and thus contaminate the detection of 21cm EOR signal. Recall that the foreground should be suppressed down to 5 orders of magnitude in the 21cm experiments. In terms of our current understanding of synchrotron self-absorption of radio galaxies and AGNs both theoretically and observationally, the spectral transition around turnover frequency should be a slowly varying physical process spanning typically a few hundreds of MHz in frequency. It seems that the soft transition model of $w \geq 200$ MHz provides a more natural and reasonable description of the spectral turnover due to synchrotron self-absorption, despite that it is only a phenomenological model.

3.4 Comparisons of angular power spectra: multi-frequencies

We can probably go one step further in exploring the effect of spectral curvature of radio sources on the multi-frequency angular power spectrum of the foregrounds. This is motivated by the widely accepted hypothesis that the cosmic 21cm signals measured at two frequencies ν and $\nu + \Delta\nu$ are uncorrelated if their frequency difference $\Delta\nu$ exceeds typically ~ 1 MHz, corresponding to a comoving scale of ~ 20 Mpc at $z = 10$, while the foregrounds beyond $\Delta\nu > 1$ MHz should still remain strongly correlated as a result of continuum radiation (e.g. Zaldarriaga, Furlanetto & Hernquist 2004; Santos, Cooray & Knox 2005; Wang et al. 2006; Datta, Choudhury & Bharadwaj 2007). Therefore, it is possible to extract the weak cosmic 21cm signal in the presence of strong foregrounds by fitting a polynomial to the multi-frequency angular power spectra $C_\ell(\nu, \nu + \Delta\nu)$ only for large intervals of $\Delta\nu$ in frequency domain and then subtracting the best-fit result from the observed $C_\ell(\nu, \nu + \Delta\nu)$. Application of this technique to the GMRT observation has been made recently by Ghosh et al. 2011a and Ghosh et al. 2011b. Equally, One can work with the three-dimensional power spectrum by removing the foreground contamination in terms of the power at lower radial component of wavenumber $k_{||}$.

Following the conventional definition, we calculate the multi-frequency angular power spectrum through $C_\ell(\Delta\nu) = C_\ell(\nu, \nu + \Delta\nu) = \langle a_{\ell m}(\nu) a_{\ell m}^*(\nu + \Delta\nu) \rangle$, where $a_{\ell m}(\nu)$ is the coefficient of spherical harmonics at frequency ν , and $\langle \cdot \cdot \cdot \rangle$ denotes the ensemble average. We take the soft transition model for description of synchrotron turnover and the same four choices of f as the above for the fraction of radio sources of spectral curvature. In Fig.10(a) we illustrate the multi-frequency angular power spectra $C_\ell(\Delta\nu)$ at $\ell = 400$ and $\ell = 1200$ derived from our simulated maps with a frequency resolution of 0.1 MHz for $\Delta\nu$ ranging from 0 to 5 MHz. We first fit a polynomial of $N_{\text{poly}} = 3$ to $C_\ell(\Delta\nu)$ over the entire frequency interval out to $\Delta\nu = 5$ MHz, and then subtract the best-fit polynomial from $\Delta\nu$ to get the corresponding residual [see Fig.10(b)] for each choice of f parameter. In all the circumstances, the residuals appear to be well below 0.1 mK, indicating that the foreground contaminations have been perfectly removed. Now we confine the polynomial fitting to the data in $\Delta\nu = 0.5$ -5 MHz. Namely, the data within $\Delta\nu = 0.5$ MHz are excluded in the fitting in order to concentrate only on the foreground contribution. The best-fit polynomials are finally subtracted from the total $C_\ell(\Delta\nu)$ over the entire range of $\Delta\nu$. It turns out that all the residuals including those in the lower frequency intervals of $\Delta\nu \leq 0.5$ MHz are smaller than 0.1 mK. Therefore, we conclude from these simple exercises that the synchrotron self-absorption of foreground radio sources has no significant influence on the construction of cosmic 21cm signal using the multi-frequency angular power spectrum technique.

4 DISCUSSION AND CONCLUSIONS

Instead of invoking a sophisticated description for the synchrotron self-absorption of extragalactic radio sources, we have taken a model characterized by three parameters to study the possible contamination of the foreground radio sources of spectral curvature in the upcoming 21cm experiments dedicated to the detection of EOR signatures: the fraction (f) of extragalactic sources whose spectral curvature occur in 100 – 1000 MHz in the restframe of the sources, the turnover frequency (ν_m) and the frequency width w that specifies the spectral transition region around ν_m . To highlight the effect of the spectral curvature, we have included neither the Milky Way foreground nor the 21 emission background of neutral hydrogen from EOR in our computations. We have used the simulated sky map of $10^\circ \times 10^\circ$ to calculate and compare the angular power spectra with and

without inclusion of the synchrotron self-absorption of extragalactic radio sources. We have then made a thorough comparison of the results between the two cases after subtracting the best-fit log-log polynomials of order $N_{\text{poly}} = 3$ on each pixel.

Presence of the synchrotron self-absorption of extragalactic radio sources breaks down the monotonically increasing/decreasing spectral feature, which may pose a challenge to the premise that the strong foreground can be perfectly removed in the 21cm experiments. It is therefore essential that the fraction, the turnover frequencies and the spectral transition profile of radio sources be robustly determined so that their influence on the 21cm experiments can be evaluated quantitatively and precisely. While the synchrotron self-absorption has been unambiguously observed in some of the radio sources especially in low frequencies ranging from 50 to 200 MHz, the above three key parameters/properties and their cosmic evolution have remained somehow uncertain so far. Our simple phenomenological model, in which the fraction (f) of the extragalactic radio sources of spectral curvature is allowed to vary, provides the first estimate of how and to what extent the synchrotron self-absorption of foreground radio sources may contaminate the measurement of the EOR signal in the 21cm experiments.

It has been shown that the effect of synchrotron self-absorption of extragalactic radio sources on the foreground removals in the 21cm experiments depends sensitively on the spectral distribution around the turnover frequency ν_m : a hard transition at ν_m leads to a sudden change of spectral index, which cannot be fitted and subtracted by the slowly varying form of polynomials. Consequently, if extragalactic radio sources whose turnover frequencies occur in the 100 – 1000 MHz waveband are not less than 0.1% of the total radio sources, the residuals of the unresolved radio foreground, manifested by either global flux or angular power spectra, would exceed the background EOR signal, increasing the difficulties of separating the cosmic EOR signatures from spectral structures of extragalactic radio sources. This is because the existence of synchrotron self-absorption characterized by the hard transition model has altered the underlying assumption about the intrinsic spectral smoothness of radio foreground along frequency space. While the hard transition model for the spectral profile of synchrotron self-absorption exaggerates the contamination of the foreground radio sources in the measurement of 21cm cosmic background, it demonstrates how foreground removals in the 21cm experiments are affected by sharp variations in the spectral profiles of radio sources even if the fraction of such radio sources is relatively small.

Theoretically, it is expected that the synchrotron self-absorption of cosmic radio sources should exhibit a smooth, rather than hard, spectral transition around turnover (e.g. O’Dell & Sartori 1970). Such a scenario is further supported by a number of radio spectral observations of QSOs, galaxies and even clusters of galaxies (e.g. Kellermann & Pauliny-Toth 1969; Laing & Peacock 1980; Andernach, Waldthausen & Wielebinski 1980; Hodges et al. 1984). This may alleviate the concern raised in the hard transition model that the effect of synchrotron self-absorption may leave pronounced imprints on the 21cm background. Indeed, using the soft transition model of $w = 200$ MHz for the radio sources of synchrotron self-absorption, we have successfully reduced the contribution of unresolved extragalactic sources to an acceptable degree ($\delta T < 1$ mK) because the smooth spectral transition spanning a few hundreds of MHz around turnover frequencies can be nicely fitted and subsequently subtracted by a set of polynomials over a frequency width of 20 MHz for each.

The presence of spectral curvature in extragalactic radio sources does increase the technical difficulties of subtracting the foreground point sources and identifying the EOR signatures. However, if the transition of spectral index for extragalactic radio sources proceeds rather smoothly around turnover frequencies as indicated presently by both physical and observational scenario, the synchrotron self-absorption of extragalactic radio sources should not constitute a major obstacle to the foreground removals for the extraction of EOR signal in the 21cm experiments. Finally, it should be noted that our calculations and results are not confined to the radio sources with synchrotron self-absorption alone but applicable to any types of radio sources of spectral curvatures, because there is no particular physics behind our phenomenological model.

5 ACKNOWLEDGMENTS

This work was supported by the Ministry of Science and Technology of China under Grant 2009CB824900, and the National Science Foundation of China under Grant 10878001/10973010/11125313. The authors would like to acknowledge an anonymous referee for constructive suggestions and insightful comments.

REFERENCES

- Andernach H., Waldthausen H., Wielebinski R., 1980, *A&AS*, 41, 339
- Bernardi G., Mitchell D. A., Ord S. M., Greenhill L. J., Pindor B., Wayth R. B., Wyithe J. S. B., 2011, *MNRAS*, 413, 411
- Bowman J. D., Rogers A. E. E., Hewitt J. N., 2007, *BAAS*, 39, 949
- Bowman J. D., Morales M. F., Hewitt J. N., 2009, *ApJ*, 695, 183
- Bowman J. D., Rogers A. E. E., 2010, *BAAS*, 42, 421
- Chapman E. et al., 2012, preprint(astro-ph/1201.2190)
- Cho J., Lazarian A., Timbie P. T., 2012, preprint(astro-ph/1203.5197)
- Cotton W. D., Uson J. M., 2008, *A&A*, 490, 455

- Datta K. K., Choudhury T. R., Bharadwaj S., 2007, MNRAS, 378, 119
- de Oliveira-Costa A., Tegmark M., Gaensler B. M., Jonas J., Landecker T. L., Reich P., 2008, MNRAS, 388, 247
- Di Matteo T., 2002, ApJ, 564, 576
- Di Matteo T., Ciardi B., Miniati F., 2004, MNRAS, 355, 1053
- Furlanetto S. R., Zaldarriaga M., Hernquist L., 2004, ApJ, 613, 1
- Furlanetto S. R., Peng Oh S., Briggs F. H., 2006, Phys. Rep., 433, 181
- Ghosh A., Bharadwaj S., Ali S. S., Chengalur J. N., 2011a, MNRAS, 411, 2426
- Ghosh A., Bharadwaj S., Ali S. S., Chengalur J. N., 2011b, MNRAS, 418, 2584
- Harker G. et al., 2010, MNRAS, 408, 2492
- Harker G. et al., 2009, MNRAS, 397, 1138
- Harker G. et al., 2010, MNRAS, 405, 2492
- Hodges M. W., Mutel R. L., Phillips R. B., 1984, AJ, 89, 1327
- Intema H. T., van der Tol S., Cotton W. D., Cohen A. S., van Bemmell I. M., Röttgering H. J. A., 2009, A&A, 501, 1185
- Jacobs D. C. et al., 2011, ApJ, 734, 34
- Jelić V. et al., 2008, MNRAS, 389, 1319
- Kellermann K. I., Pauliny-Toth I. I. K., 1969, ApJ, 155
- Knox L., Cooray A., Eisenstein D., Haiman Z., 2001, ApJ, 550, 7
- Laing R. A., Peacock I. A., 1980, MNRAS, 190, 903
- Liu A., Tegmark M., 2011, Phys. Rev. D, 83, 103006
- Liu A., Tegmark M., Bowman J., Hewitt J., Zaldarriaga M., 2009, MNRAS, 398, 401
- Morales M. F., Wyithe J. S. B. 2010, ARA&A, 48, 127
- Noordam J. E., 2004, SPIE, Proceedings of the SPIE, 5489, 817
- O'Dell S. L., Sartori L., 1970, ApJ, 162, 37
- Pacholczyk A. G., 1970, ApJ, 161, 207
- Petrovic N., Peng Oh S., 2011, MNRAS, 413, 2103
- Pritchard J. R., Loeb A., 2010, Phys. Rev. D, 82, 023006
- Pritchard J. R., Loeb A., 2011, preprint(astro-ph/1109.6012)
- Santos M. G., Cooray A., Knox L., 2005, ApJ, 625, 575
- Schwab F. R., 1984, AJ, 89, 1076
- Steppe H., Jeyakumar S., Saikia D. J., Salter C. J., 1995, A&AS, 113,409
- Singal J., Stawarz L., Lawrence A., Petrosian V., 2010, MNRAS, 409, 1172
- Tsvetanov Z. I., Charugin V. M., 1981, SvA, 25, 293
- Van del Tol S., Jeffs B. D., van der Veen A. -J., 2007, IEEE Transactions on Signal Processing, 55, 9
- Vernstrom T., Scott D., Wall J. V., 2011, MNRAS, 415, 3641
- Wang X., Tegmark M., Santos M. G., Knox L., 2006, ApJ, 650, 529
- Wang J. et al., 2010, ApJ, 723, 620
- Wilman R. J. et al., 2008, MNRAS, 388, 1335
- Zaldarriaga M., Furlanetto S. R., Hernquist L., 2004, ApJ, 608, 622

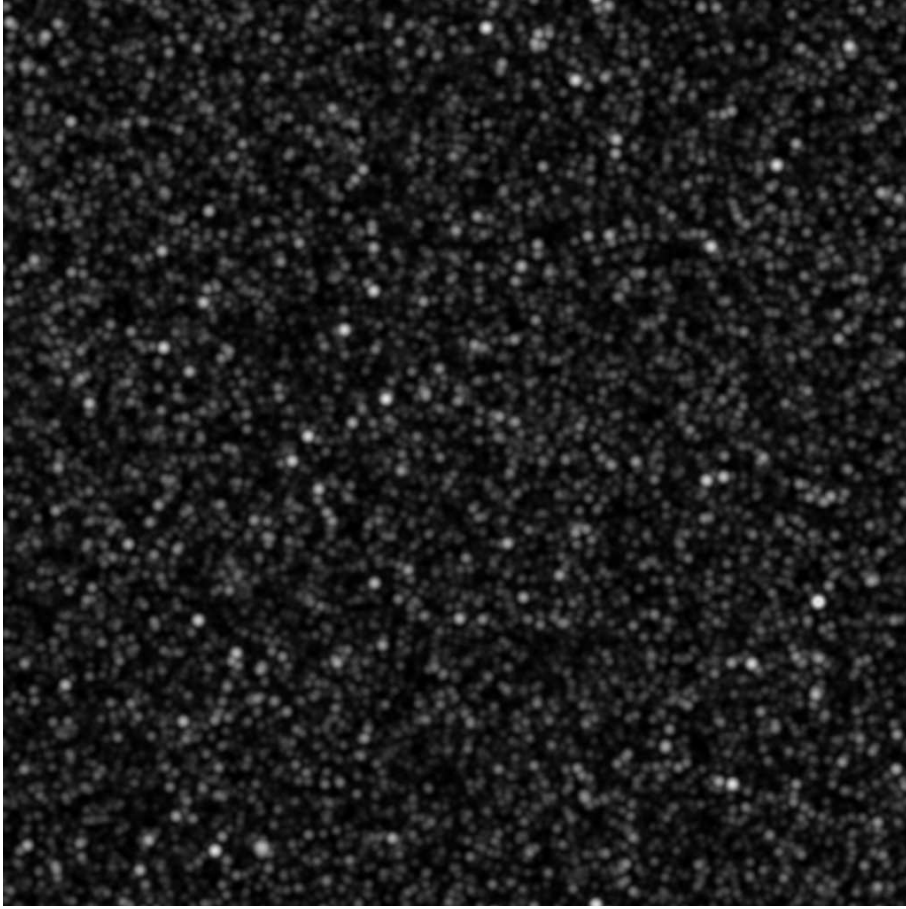


Figure 1. Simulated sky map of the 'unresolved' radio sources below 100 mJy at frequency $\nu = 150$ MHz. The map has an angular size of $10^\circ \times 10^\circ$ and is smoothed with a Gaussian kernel of FWHM= $1'.98$.

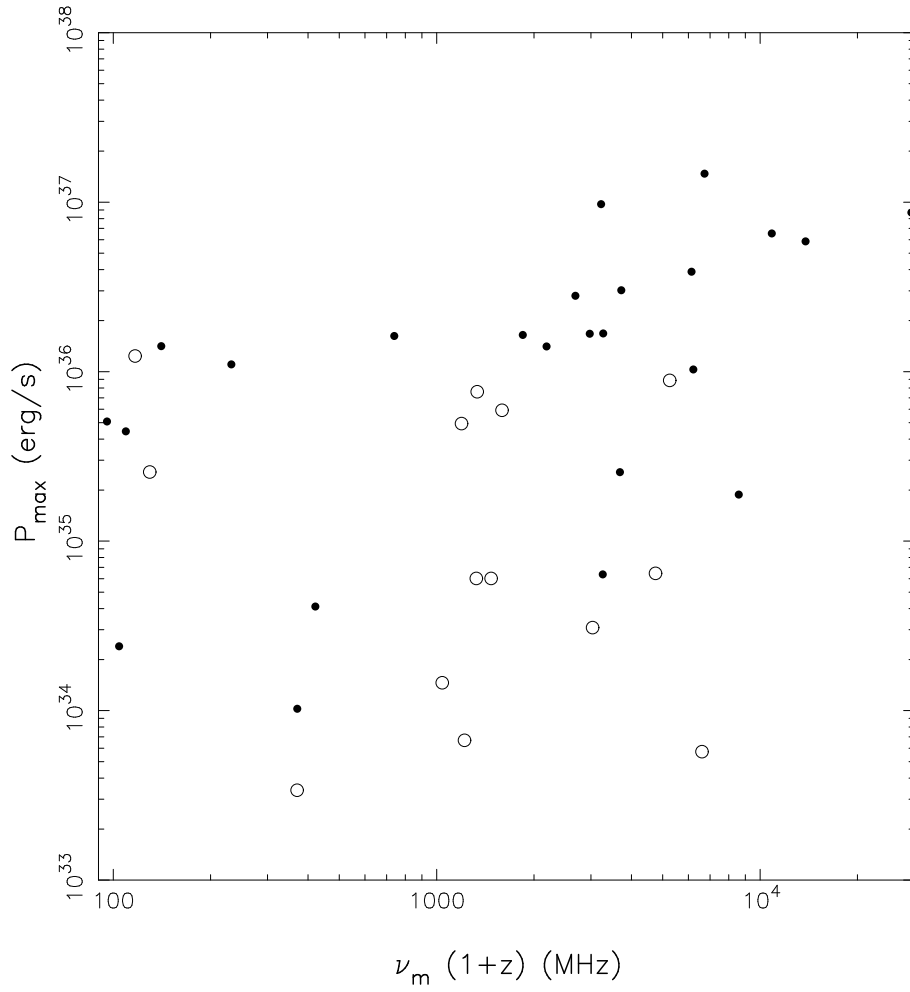


Figure 2. Peak radio luminosities P_{max} are plotted against turnover frequencies $\nu_m(1+z)$ for 39 radio sources in which the spectral curvatures are successfully interpreted as being due to synchrotron self-absorption. Data are compiled from Kellermann & Pauliny-Toth (1969), Hodges et al. (1984) and Steppe et al. (1995). Galaxies and AGNs are denoted by open and filled circles, respectively.

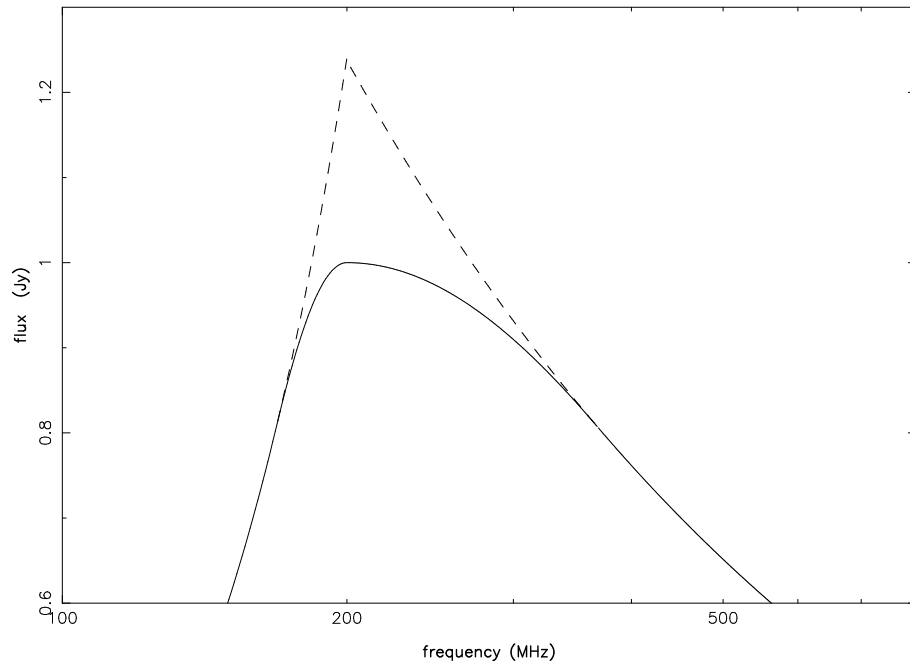


Figure 3. An example of the hard transition model (dashed line) and the soft transition model of $w = 200$ MHz (solid line) at $\nu_m = 200$ MHz.

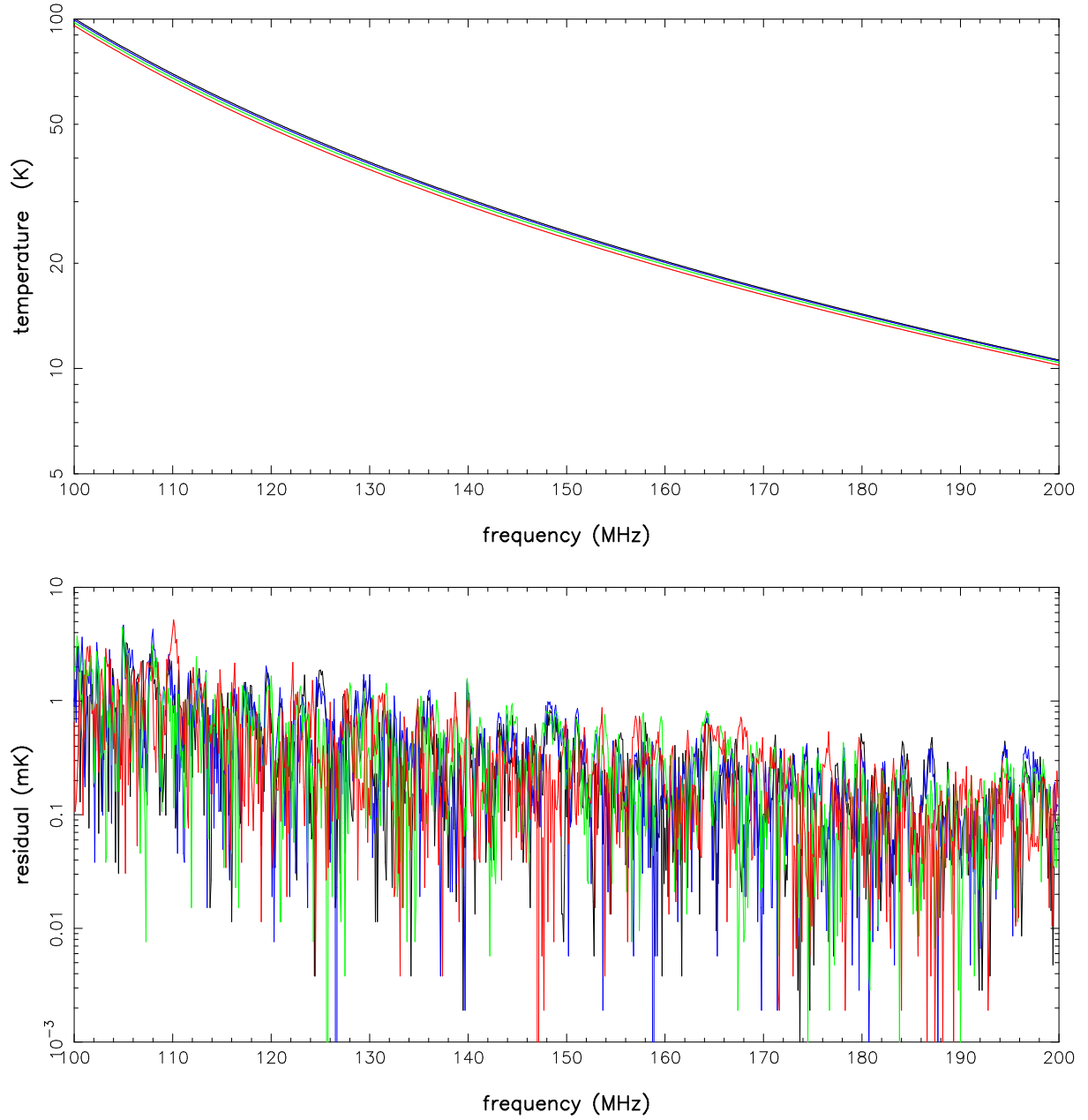


Figure 4. Top panel: Average surface brightness temperature versus frequency for four choices of f , the fraction of radio sources with turnover frequencies in 100-1000 MHz range: $f = 10\%$ (red line), $f = 1\%$ (green line), $f = 0.1\%$ (blue line), and $f = 0\%$ (black line). Bottom panel: The corresponding residuals for the four models of f after the best-fitted polynomials of $N_{\text{poly}} = 3$ are subtracted.

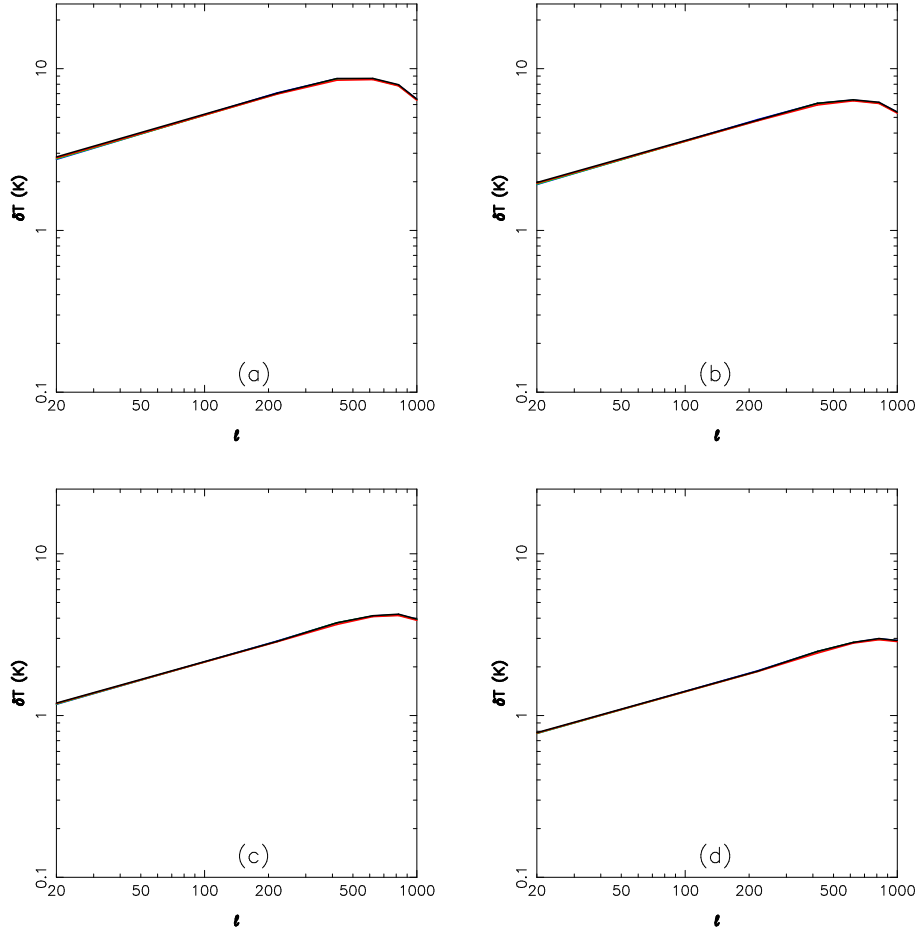


Figure 5. Angular power spectra of the 'unresolved' foregrounds down to $S_{150\text{MHz}} = 100$ mJy for the four models of f and at four frequencies: (a) $\nu = 110$ MHz, (b) $\nu = 125$ MHz, (c) $\nu = 150$ MHz and (d) $\nu = 175$ MHz. The power spectra, represented by $\delta T = [\ell(2\ell + 1)C_\ell/4\pi]^{1/2}$, are dominated by the shot noises of the radio sources and rather insensitive to the choice of f .

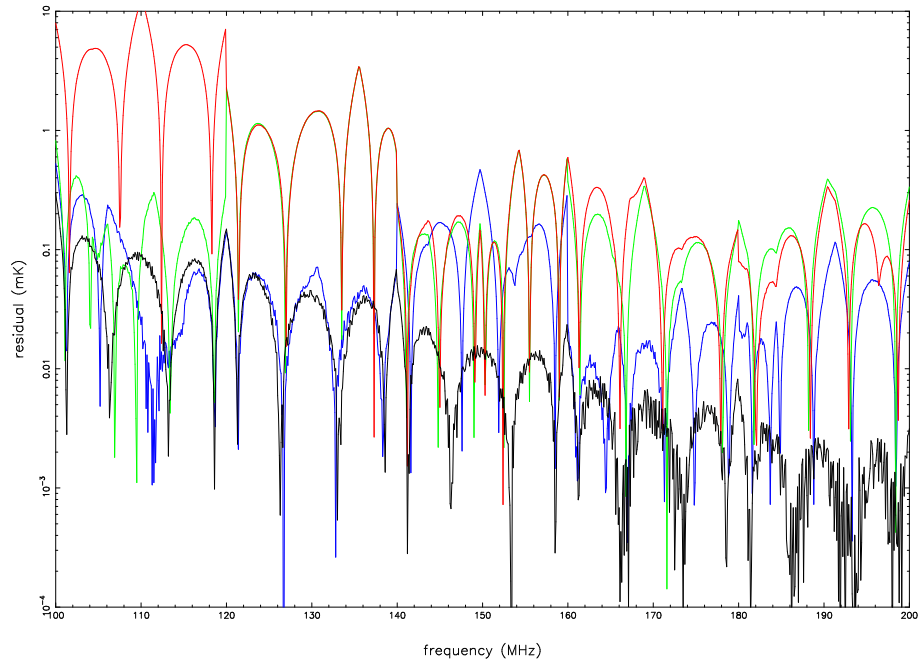


Figure 6. Average surface brightness temperature of the residual maps after the best-fit polynomials over a bandwidth of 20 MHz are subtracted on each pixel for the hard transition model. The same notations as in Fig.4 are adopted.

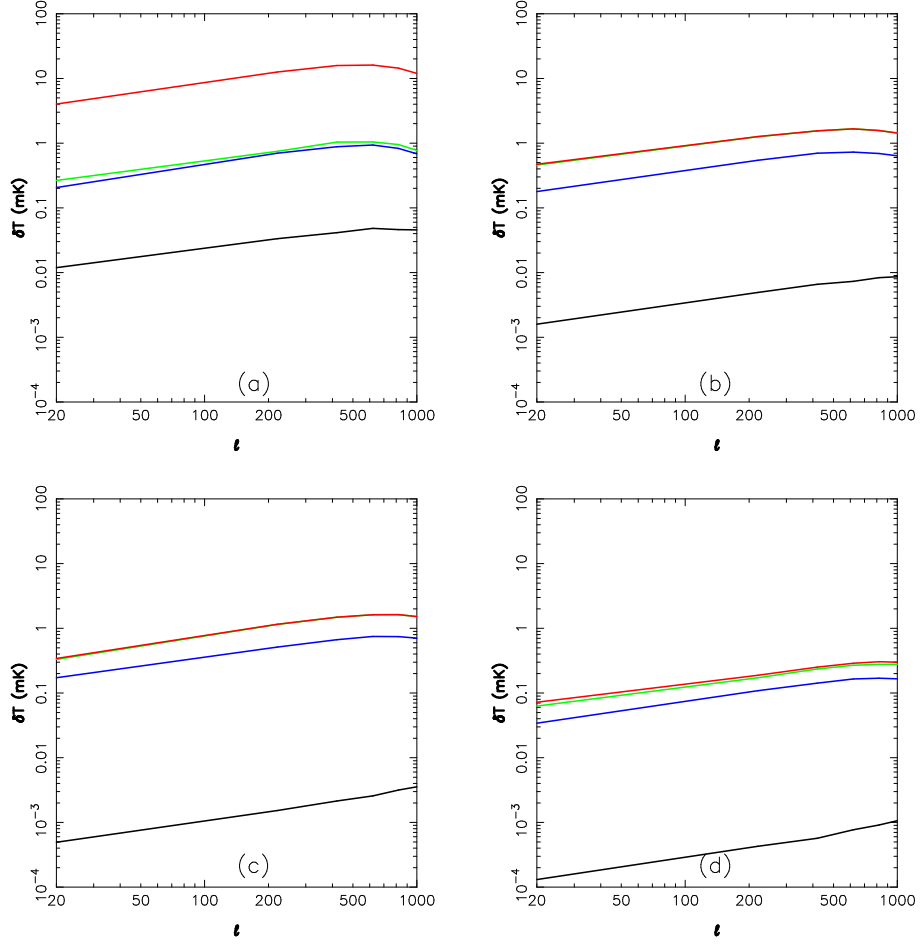


Figure 7. Angular power spectra of the residual maps, corresponding to the four plots in Fig.5, after subtracting the best-fitted polynomials on each pixel. The same notations as in Fig. 4 are shown for the four models of f .

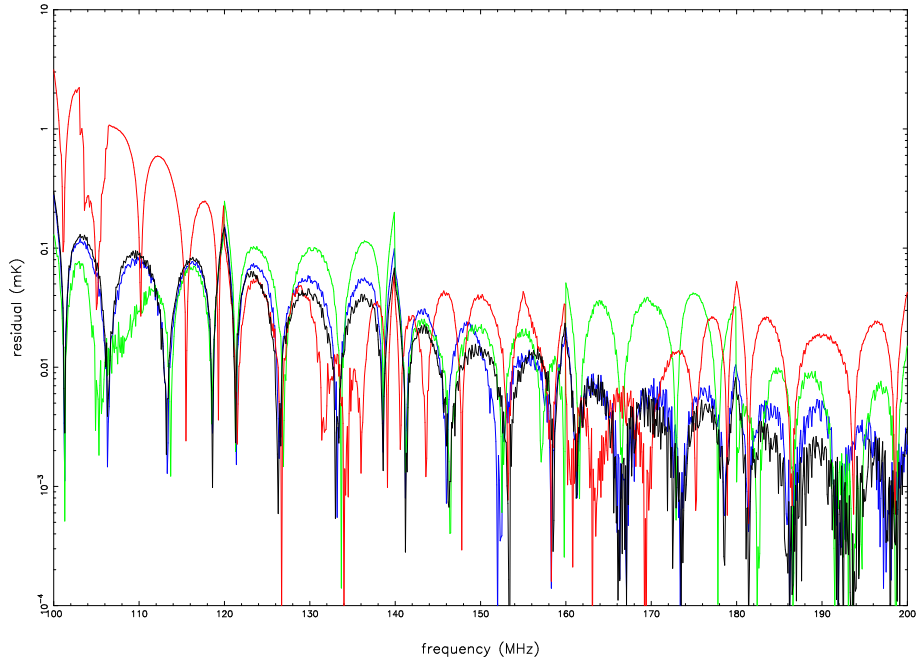


Figure 8. The same as Fig. 6 but for the soft transition model of $w = 200$ MHz.

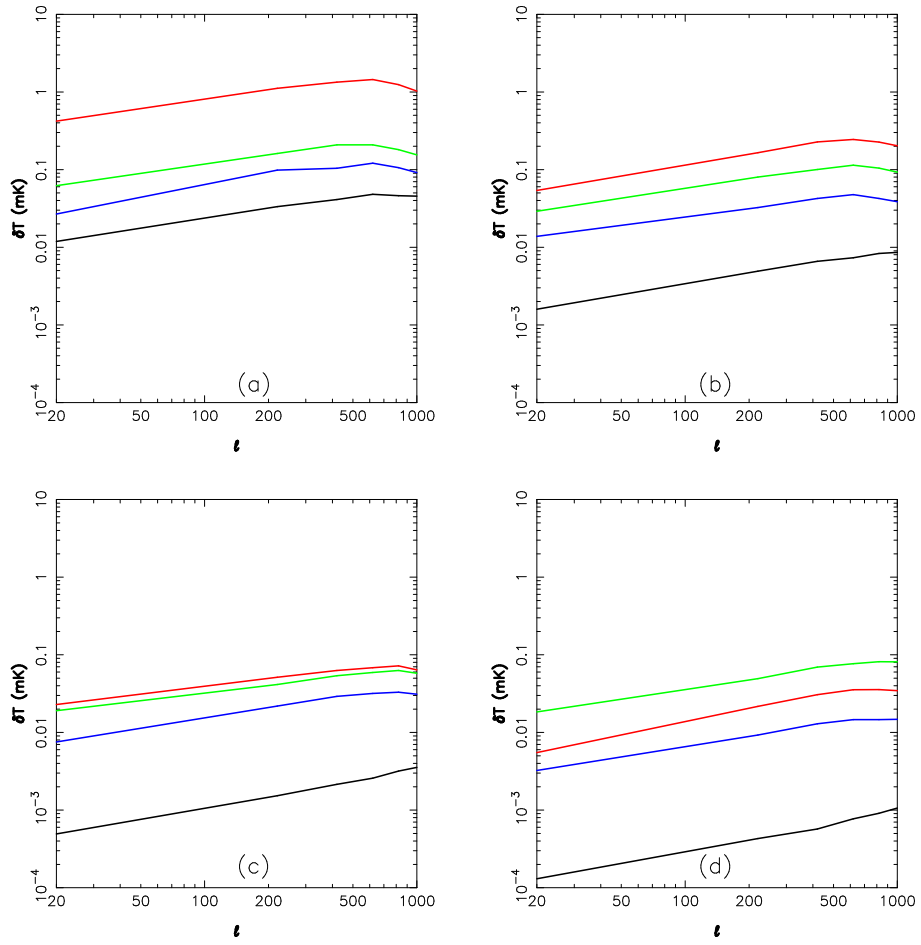


Figure 9. The same as Fig. 7 but for the soft transition model of $w = 200$ MHz.

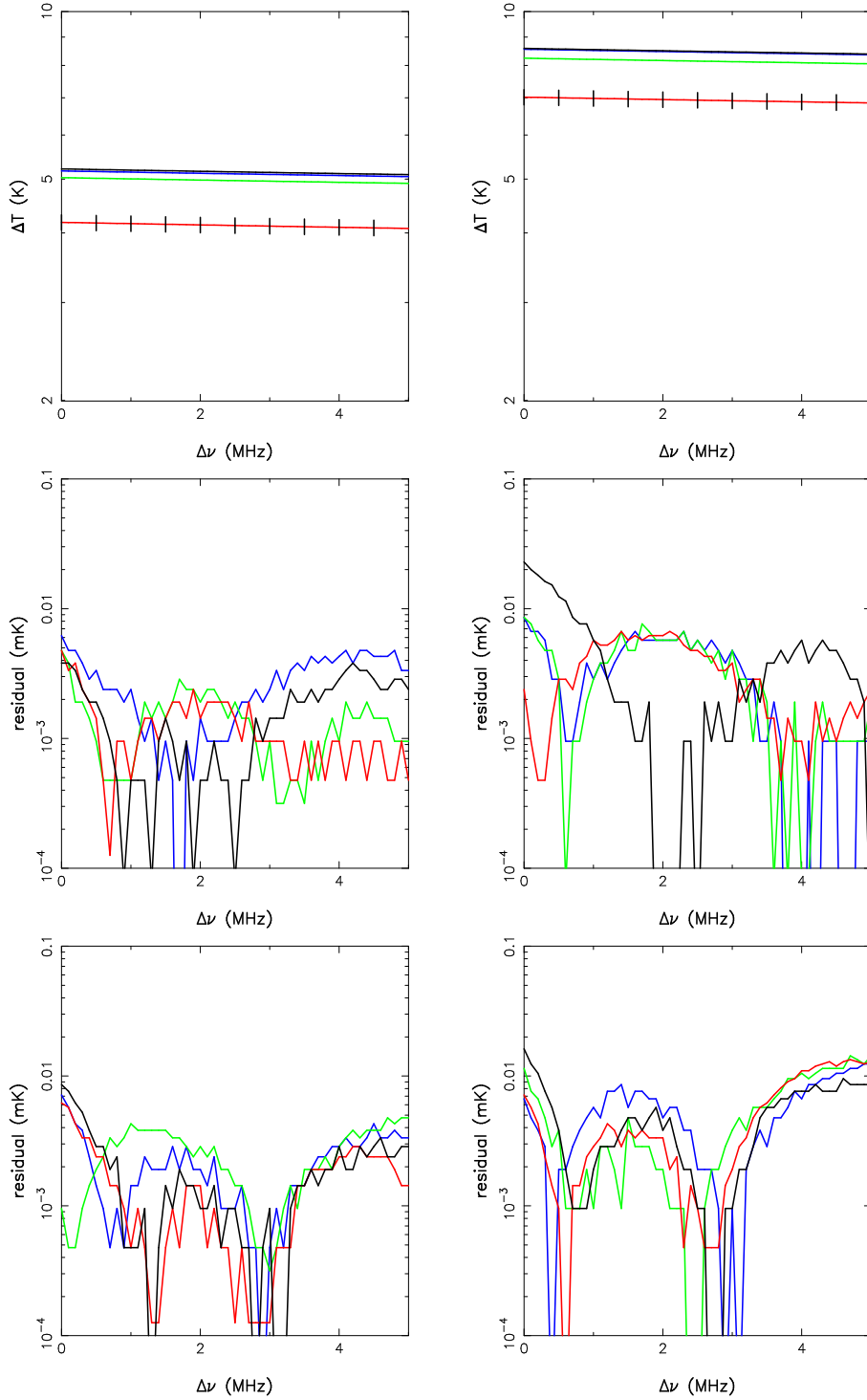


Figure 10. Top panels: The multi-frequency angular power spectra against frequency interval $\Delta\nu$ for soft transition model, which are represented by $\Delta T = [\ell(2\ell + 1)C_\ell(\Delta\nu)/4\pi]^{1/2}$; Middle panels: The residuals in ΔT after the best-fit polynomials in the frequency intervals of 0-5 MHz are subtracted; Bottom panels: The residuals in ΔT after the best-fit polynomials in the frequency intervals of 0.5-5 MHz are subtracted. Left and right panels correspond to $\ell = 400$ and $\ell = 1200$, respectively. The same colours as in Fig.4 are used to denote the different choices of f parameters. We have illustrated, for the case of $f = 10\%$, the typical statistical errors associated with the multi-frequency angular power spectra.